Yukawa corrections to charged Higgs-boson pair production in photon-photon collisions

Ma Wen-Gan
China Center of Advanced Science and Technology (World Laboratory), P.O. Box 8730, Beijing 100080, People's Republic of China
and Modern Physics Department, University of Science and Technology of China, Anhui 230027, People's Republic of China

Chong-Sheng Li
China Center of Advanced Science and Technology (World Laboratory), P.O. Box 8730, Beijing 100080, People's Republic of China
and Physics Department, Peking University, Beijing 100871, People's Republic of China

Han Liang
Modern Physics Department, University of Science and Technology of China, Anhui 230027, People's Republic of China
(Received 10 July 1995)

We study the $O(\alpha m_t^2/m_W^2)$ Yukawa corrections to the process $e^+e^- \to \gamma\gamma \to H^+H^-$ at the Next Linear Collider. The analyses of the production rate are made in the framework of the two-Higgs-doublet model for possible parameter values of the Higgs sector. We find that the corrections imply a few to 22% reduction in the production cross section in e^+e^- colliders.

PACS number(s): 14.80.Cp, 12.15.Lk, 12.60.Cn

I. INTRODUCTION

Until now, all the precision data from the CERN Large Electron-Positron Collider (LEP) and SLAC Linear Collider (SLC) have confirmed the minimal standard model (MSM) [1,2]. However, to completely establish the MSM not only is the precise measurement of the parameters of particle physics needed, but also the direct discovery of the MSM predicted particles is needed. Direct evidence for the top quark was recently presented by the Collider Detector at Fermilab (CDF) Collaboration [3]. The absence of Higgs-boson signal events leads to a lower bound $m_{H^0} > 63.5$ GeV at 95% C.L. [4]. If these two particles are directly verified, this will be a great success for the standard model. Because of their large masses, the multi-TeV hadron colliders such as the Fermilab Tevatron and the CERN Large Hadron Collider (LHC) are expected to be devoted to the precise characters of the Higgs sector and top quark. In addition to providing the first evidence for the top quark or Higgs boson, the multi-TeV collider offers the possibility of carrying on the research of other unknown particles in the hitherto unexplored mass range. There has been a great deal of theoretical and phenomenological interests in one such new particle: i.e., the charged Higgs boson [5] appearing in the two-Higgs-doublet model (THDM) [6]. It is because of this that the extension of the MSM, which includes a second Higgs doublet, is far from being ruled out experimentally at present and is another strong motivation for extending the Higgs sector into two Higgs doublets; this comes from the fact that it has a common feature of many extensions of the MSM, such as the minimal supersymmetric standard model (MSSM). The MSSM model requires two SU(2) doublets to give masses to up and down quarks [5]. Therefore one expects an observable signal throughout the allowed range of the coupling parameter $\tan\beta$.

The Next Linear Collider (NLC) operating at a center-of-mass energy of 500–2000 GeV with a luminosity of the order of 10^{33} cm^{-2} s^{-1} may produce a charged Higgs boson pair with an observable production rate, since the events would be much cleaner than in pp and $p\bar{p}$ colliders and the parameters of the charged Higgs boson would be easier to extract. Nowadays, the new possibility of $\gamma\gamma$ collisions at the linear e^+e^- collider deserves a lot of attention. With the advent of the new collider technique [7], the high energy and high intensity photon beams will be obtained by using Compton laser photons scattering off the colliding electron and positron beams. The luminosity and energy of colliding photons are expected to be comparable to that of the primary e^+e^- collisions. Thus it offers another possible way to produce new particles directly. This mechanism can be employed at the NLC.

The THDM contains six parameters: two scalar neutral Higgs bosons masses m_{H^0} and m_{h^0}, one neutral pseudoscalar Higgs boson mass m_{A^0}, one pair of charged Higgs boson masses $m_{H^\pm}$, and the additional mixing angle α and β. α describes the mixing angle of the scalar Higgs bosons H^0 and h^0. β is defined as the mixing parameter of charged and pseudoscalar Higgs bosons which is related directly to the vacuum expectation values of Higgs doublets. The definition of β is $\tan\beta = v_2/v_1$ [6].

In this paper we calculate the cross section of charged Higgs boson pair production through $\gamma\gamma$ collision in an e^+e^- collider including the $O(\alpha m_t^2/m_W^2)$ Yukawa corrections in a two-Higgs-doublet model. The lowest order calculation for this process has been already done by

Bowser-Chao *et al.* [8]. As we know, in the lowest order this process is model independent because the γH^+H^- coupling is universal. The calculation of this process with Yukawa corrections however, is model dependent. In our calculation, we keep the convention that the up-type (down-type) quarks couple only to the vacuum expectation value $v_2(v_1)$, so that the model has the same Yukawa coupling structure with the MSSM model.

The paper is organized as follows: The lowest order cross section and the details of the $O(\alpha m_t^2/m_W^2)$ Yukawa corrections are given in Sec. II. In Sec. III there are numerical results and discussion. Finally a short summary is in Sec. IV.

II. CALCULATION

The Feynman diagrams for the process $\gamma\gamma \to H^+H^-$, which include the $O(\alpha m_t^2/m_W^2)$ Yukawa corrections, are depicted in Figs. 1–4. The tree-level diagrams are shown in Fig. 1. The self-energy, vertex, and box correction diagrams are in Figs. 2, 3, and 4, respectively. In our calculation we used the 't Hooft–Feynman gauge. All the ultraviolet divergences are eliminated by dimensional regularization and the complete on-mass-shell (COMS) renormalization scheme [9]. In the COMS scheme, the usual on-mass-shell condition and the coupling constant renormalization are adopted and the fields are renormalized in such a way that the residues of all renormalized propagators are equal to one. The renormalized amplitude for process $\gamma\gamma \to H^+H^-$ is given by

$$M_{\rm ren} = M_0 + \delta M^{\rm self} + \delta M^{\rm vert} + \delta M^{\rm box} \tag{1}$$

where M_0 is the amplitude at the tree level, $\delta M^{\rm self}$, $\delta M^{\rm vert}$, and $\delta M^{\rm box}$ are the $O(\alpha m_t^2/m_W^2)$ Yukawa corrections arising from the self-energy, vertex, and box diagrams, respectively.

(1) The lowest order matrix elements. The relevant Feynman diagrams at the tree level are shown in Fig. 1 and the Feynman rules can be found in Ref. [10]. The corresponding amplitude at the lowest order for $\gamma\gamma \to H^+H^-$ is given by

$$M_0 = M_0^t + M_0^u + M_0^q \tag{2}$$

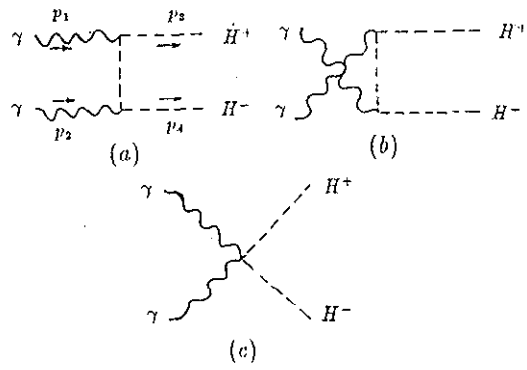

FIG. 1. The tree-level diagram of subprocess $\gamma\gamma \to H^+H^-$.

where M_0^t, M_0^u, and M_0^q represent the amplitudes of the t-channel, u-channel, and quartic coupling diagrams in Fig. 1, respectively. Their explicit expressions can be given as

$$M_0^t = \frac{ie^2}{\hat{t} - m_{H^\pm}^2}(p_2 - 2p_4)^\nu \epsilon_\nu(p_2)(p_2 + p_3 - p_4)^\mu \epsilon_\mu(p_1) , \tag{3}$$

$$M_0^u = \frac{-ie^2}{\hat{u} - m_{H^\pm}^2}(p_1 - 2p_4)^\mu \epsilon_\mu(p_1)(p_1 + p_3 - p_4)^\nu \epsilon_\nu(p_2) , \tag{4}$$

$$M_0^q = 2ie^2 g^{\mu\nu}\epsilon_\mu(p_1)\epsilon_\nu(p_2) . \tag{5}$$

The Mandelstam variables $\hat{t}$ and $\hat{u}$ are defined as $\hat{t} = (p_2 - p_4)^2, \hat{u} = (p_1 - p_4)^2$. As shown in Fig. 1, there p_1 and p_2 denote the momenta of incoming photons and p_3 and p_4 represent the momenta of the outgoing two charged Higgs bosons.

(2) Self-energy corrections. The self-energy corrections at the $O(\alpha m_t^2/m_W^2)$ level arising from the t-, u-channel, and quartic interaction graphs are drawn in Fig. 2. In the COMS scheme, the contributions from graphs with external self-energies [shown in Figs. 2(1,2), 2(3,4), and 2(7,8)] are canceled by the corresponding counterterm graphs. The internal charge Higgs self-energy $\Sigma^{H^+H^+}$ arising from the diagram in Fig. 2(5,6) contributes to the one-loop amplitude with

$$\delta M^{\rm self} = -M_0^t\left[\frac{\Sigma^{H^+H^+}(\hat{t}) - \delta m_{H^\pm}^2}{\hat{t} - m_{H^\pm}^2} + \delta Z_{H^\pm}^2\right] - M_0^u\left[\frac{\Sigma^{H^+H^+}(\hat{u}) - \delta m_{H^\pm}^2}{\hat{u} - m_{H^\pm}^2} + \delta Z_{H^\pm}^2\right] , \tag{6}$$

where the unrenormalized self-energy function of the charged Higgs boson $\Sigma^{H^+H^+}$ represents only the part to the order $O(\alpha m_t^2/m_W^2)$. It has the form

$$\Sigma^{H^+H^+}(k^2) = \frac{-N_c}{4\pi^2}\{(g_+^2 + g_-^2)[A_0(m_t^2) - m_b^2 B_0 - k^2 B_1] - (g_+^2 - g_-^2)m_b m_t B_0\}[k^2, m_b^2, m_t^2] , \tag{7}$$

where N_c is the number of colors, and the definitions of one-point and two-point functions A_0 and B_0 are adopted from Ref. [11]. The arguments of B functions are written at the end of the formulas in parentheses. The g_+ and g_- are defined in the coupling constant of H^+tb as

$$g_{H^+tb} = g_+ + g_-\gamma_5 = \frac{ig}{2\sqrt{2}m_W}[(m_b \tan\beta + m_t \cot\beta) + (m_b \tan\beta - m_t \cot\beta)\gamma_5] . \tag{8}$$

The renormalization conditions allow to express the renormalization constants of $\delta m_{H^\pm}$ and $\delta Z_{H^\pm}$ by the unrenormalized self-energies at special external momenta:

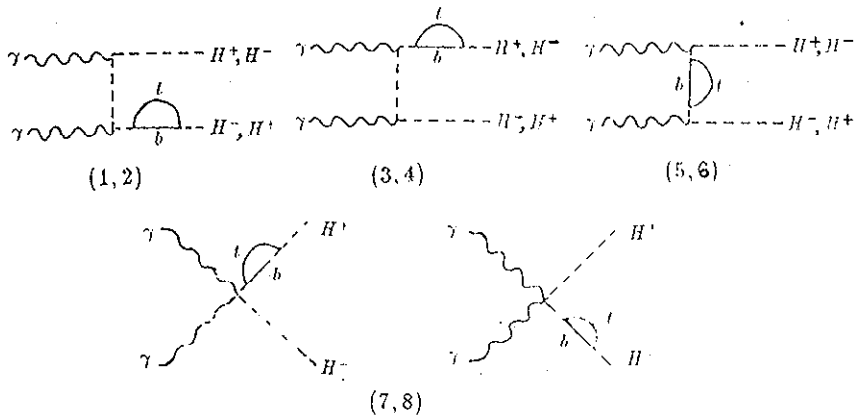

FIG. 2. The self-energy correction diagrams of subprocess $\gamma\gamma \to H^+H^-$ to $O(\alpha m_t^2/m_W^2)$.

$$\delta m_{H^\pm}^2 = \mathrm{Re}\Sigma^{H^+H^+}(m_{H^\pm}^2) ,$$

$$\delta Z_{H^\pm} = -\left.\frac{\partial \Sigma^{H^+H^+}(k^2)}{\partial k^2}\right|_{k^2=m_{H^\pm}^2} . \tag{9}$$

(3) Vertex corrections. The vertex corrections include the eight diagrams shown in Fig. 3. Their analytical expressions are written as

$$\begin{aligned}\delta M^{\mathrm{vert}} = -ie^2\epsilon^\mu(p_1)\epsilon^\nu(p_2)\Bigg[&\frac{(p_2-2p_4)_\nu}{\hat{t}-m_{H^\pm}^2}(f_1+f_5)_\mu + \frac{(p_2+p_3-p_4)_\mu}{\hat{t}-m_{H^\pm}^2}(f_3+f_7)_\nu \\ &+\frac{(p_1+p_3-p_4)_\mu}{\hat{u}-m_{H^\pm}^2}(f_2+f_6)_\mu\frac{(p_1-2p_4)_\mu}{\hat{u}-m_{H^\pm}^2}(f_4+f_8)_\nu\Bigg] \\ &+(M_0^t+M_0^u)\left(\delta Z_e+\frac{1}{2}\delta Z_{AA}+\frac{s_W^2-c_W^2}{2s_Wc_W}\frac{1}{2}\delta Z_{ZA}+\delta Z_{H^\pm}\right) .\end{aligned} \tag{10}$$

The explicit expressions of form factors $f_{i\mu}$ $(i = 1\text{–}8)$ are presented in the Appendix. They correspond to the correction (parts 1–8) of the diagram in Fig. 3 respectively. The charge and wave-function renormalization constants can be deduced from the formulas of Ref. [11] and Eqs. (7)–(9). The following expressions from Ref. [11] are used here:

$$\delta Z_e = \frac{1}{2}\left.\frac{\partial\Sigma_T^{AA}(k^2)}{\partial k^2}\right|_{k^2=0} - \frac{s_W}{c_W}\frac{\Sigma_T^{AZ}(0)}{m_Z^2} , \tag{11}$$

$$\delta Z_{AA} = -\left.\frac{\partial\Sigma_T^{AA}(k^2)}{\partial k^2}\right|_{k^2=0} , \tag{12}$$

$$\delta Z_{ZA} = 2\frac{\Sigma_T^{AZ}(0)}{m_Z^2} . \tag{13}$$

The self-energy parts concerned in our evolution, which contain only the contributions to the order $O(\alpha m_t^2/m_W^2)$, can be extracted from their full expression in Refs. [11,12]. They have the expressions as

$$\begin{aligned}\Sigma^{ZA}(k^2) = &\frac{\alpha}{3\pi}\frac{3-8s_W^2}{6s_Wc_W}\left(-(k^2+2m_t^2)B_0[k^2,m_t^2,m_t^2]+2m_t^2B_0[0,m_t^2,m_t^2]+\frac{k^2}{3}\right) \\ &+\frac{\alpha}{4\pi}\frac{s_W^2-c_W^2}{6s_Wc_W}\left((k^2-4m_{H^\pm}^2)B_0[k^2,m_{H^\pm}^2,m_{H^\pm}^2]-4m_{H^\pm}^2B_0[0,m_{H^\pm}^2,m_{H^\pm}^2]+\frac{2k^2}{3}\right) ,\end{aligned} \tag{14}$$

$$\begin{aligned}\Sigma_T^{AA}(k^2) = &-\frac{4\alpha}{9\pi}\left(-(k^2+2m_t^2)B_0[k^2,m_t^2,m_t^2]+2m_t^2B_0[0,m_t^2,m_t^2]+\frac{k^2}{3}\right) \\ &+\frac{\alpha}{12\pi}\left((k^2-m_{H^\pm}^2)B_0[k^2,m_{H^\pm}^2,m_{H^\pm}^2]-4m_{H^\pm}^2B_0[0,m_{H^\pm}^2,m_{H^\pm}^2]+\frac{2k^2}{3}\right) .\end{aligned} \tag{15}$$

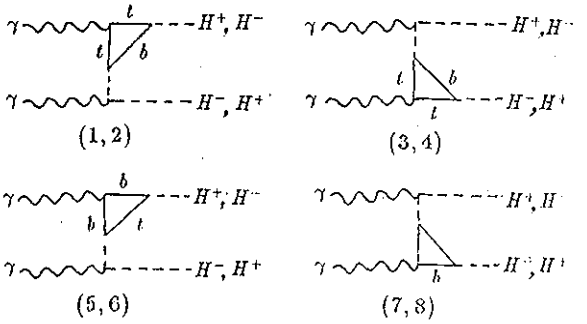

FIG. 3. The vertex diagrams of subprocess $\gamma\gamma \to H^+H^-$ to order $O(\alpha m_t^2/m_W^2)$.

(4) Box corrections. The box graphs are shown in Fig. 4. They yield the correction amplitude expressed as

$$\delta M^{\rm box} = 2ie^2 g_{\mu\nu}\epsilon^\mu(p_1)\epsilon^\nu(p_2) \times\left(f_9+f_{10}+f_{11}+f_{12}+f_{13}+f_{14}+2\delta Z_e +\delta Z_{AA}+\frac{s_W^2-c_W^2}{4s_Wc_W}\delta Z_{ZA}+\delta Z_{H^\pm}\right) . \quad (16)$$

The form factors f_i $(i = 9$–$14)$ are given by the box diagrams 1–6 in Fig. 4, respectively. Their explicit expressions are also listed in the Appendix. The corresponding amplitude squared for subprocess $\gamma\gamma \to H^+H^-$ can be written as

$$\overline{\sum}|M_{\rm ren}|^2 = \overline{\sum}|M_0|^2 +2\,{\rm Re}\overline{\sum}(\delta M^{\rm self}+\delta M^{\rm vert}+\delta M^{\rm box})M_0^\dagger , \quad (17)$$

where the bar over the summation recalls averaging over initial spins. The total cross section is given by

$$\hat\sigma(\hat s) = \frac{1}{16\pi\hat s^2}\int_{\hat t-}^{\hat t+} d\hat t\overline{\sum}|M_{\rm ren}(\hat s,\hat t)|^2 , \quad (18)$$

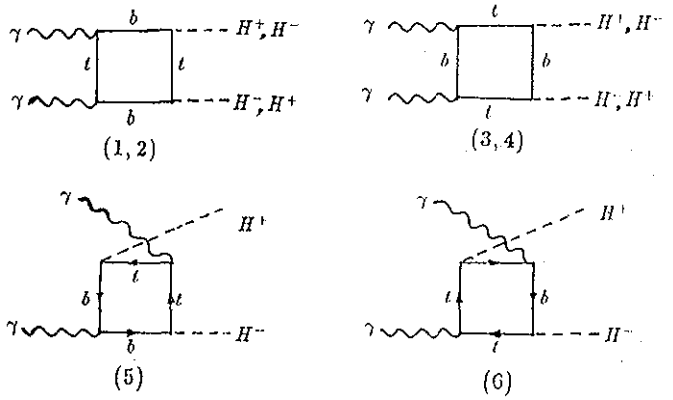

FIG. 4. The box diagrams of subprocess $\gamma\gamma \to H^+H^-$ to order $O(\alpha m_t^2/m_W^2)$.

where $\hat t^\pm = (m_{H^\pm}^2 - s/2) \pm \hat s\beta_{H^\pm}/2$ and $\beta_{H^\pm} = \sqrt{1-4m_{H^\pm}^2/\hat s}$. The total cross section for the charged Higgs pair production in the e^+e^- collider can be obtained by folding the $\hat\sigma$, the cross section of the subprocess $\gamma\gamma \to H^+H^-$, with the photon luminosity:

$$\sigma(s) = \int_{2m_{H^\pm}/\sqrt{s}}^{x_{\rm max}} dz\frac{dL_{\gamma\gamma}}{dz}\hat\sigma(\gamma\gamma \to H^+H^+ \text{ at } \hat s = z^2 s) , \quad (19)$$

where $\sqrt{s}$ and $\sqrt{\hat s}$ are the e^+e^- and $\gamma\gamma$ center-of-mass energies respectively and the quantity $dL_{\gamma\gamma}/dz$ is the photon luminosity, which is defined as

$$\frac{dL_{\gamma\gamma}}{dz} = 2z\int_{z^2/x_{\rm max}}^{x_{\rm max}}\frac{dx}{x}F_{\gamma/e}(x)F_{\gamma/e}(z^2/x) . \quad (20)$$

For unpolarized initial electrons and a laser, the energy spectrum of the backscattered photon is given by [13]

$$F_{\gamma/e}(x) = \frac{1}{D(\xi)}\left[1-x+\frac{1}{1-x}-\frac{4x}{\xi(1-x)} +\frac{4x^2}{\xi^2(1-x)^2}\right] , \quad (21)$$

where

$$D(\xi) = \left(1-\frac{4}{\xi}-\frac{8}{\xi^2}\right)\ln(1+\xi)+\frac{1}{2}+\frac{8}{\xi}-\frac{1}{2(1+\xi)^2} , \quad (22)$$

and $\xi = 4E_0\omega_0/m_e^2$, m_e, and E_0 are the mass and energy of the incident electron, respectively, and ω_0 is the laser-photon energy. The dimensionless parameter x represents the fraction of the energy of the incident electron carried by the backscattered photon. In our evaluation, we choose ω_0 such that it maximizes the backscattered photon energy without spoiling the luminosity through e^+e^- pair creation. Then we can get $\xi = 2(1+\sqrt{2}) \simeq 4.8$, $x_{\rm max} \simeq 0.83$, and $D(\xi) \simeq 1.8$. That is a usual method which was used in Refs. [8,14].

III. NUMERICAL RESULTS AND DISCUSSION

In the one-loop calculation, the physical mass eigenstates of the particles concerned and the renormalized constants are fixed by the conditions that the input parameters m_W, m_Z, m_{H^0}, m_{h^0}, m_{A^0}, and $m_{H^\pm}$ are the physical masses. But those masses are not all independent, m_W can be determined if we specified the m_Z and Higgs boson masses by the well-known μ decay constant G_μ:

$$m_W^2\left(1-\frac{m_W^2}{m_Z^2}\right) = \frac{\pi\alpha}{\sqrt{2}G_F(1-\Delta r_{\rm THDM})} . \quad (23)$$

Then a more precise value of m_W and thus s_W are obtained and the lowest-order cross section depends on m_t

and the Higgs boson masses. In the G_F scheme, α, G_F, and m_Z are used as input parameters and m_W is determined through Eq. (23), where $\Delta r_{\rm THDM}$ includes all the weak radiative corrections to muon decay in the THDM frame. The quantity of $\Delta r_{\rm THDM}$ can be expressed as [15]

$$\Delta r_{\rm THDM} = \Delta r_{\rm MSM} + \Delta r_{\rm NS} , \tag{24}$$

where the $\Delta r_{\rm MSM}$ is the sum of the standard corrections [16] and the nonstandard correction part $\Delta r_{\rm NS}$ has the quantitative equation [15]

$$\Delta r_{\rm NS} = \frac{1}{m_W^2}[\Sigma_{T,\rm NS}^{WW}(0) - {\rm Re}\Sigma_{T,\rm NS}^{WW}(m_W^2)] - \frac{c_W^2}{s_W^2}\left(\frac{\delta m_Z^2}{m_Z^2} - \frac{\delta m_W^2}{m_W^2}\right) + \frac{\alpha}{12\pi}\ln\frac{m_W^2}{m_{H^\pm}^2} , \tag{25}$$

where the self-energy function $\Sigma_{T,\rm NS}^{WW}$ represents the nonstandard part of self-energy function Σ_T^{WW} in THDM. In the numerical evaluation we use the G_F scheme and take a set of independent input parameters which is known from current experiments [17]. They are $\alpha = 1/137.035\,989\,5$, $G_F = 1.166\,392 \times 10^{-5}$ GeV^{-2}, $m_Z = 91.1888$ GeV, $m_t = 175$ GeV, and $m_b = 4.7$ GeV.

The experiment constraints from LEP [18], CP violation, K and B physics [19], and unitarity and perturbativity considerations [20] give the following limitations on the parameters of THDM:

$$0.5 \le \tan\beta \le 100, 0 < m_{h^0}, m_{A^0} \le 1 \text{ TeV} ,$$

$$m_{H^\pm} \ge \frac{1}{2}m_Z . \tag{26}$$

The recent literature shows also that high energy constraints derived from the W mass, the full width of the Z boson, and the $b\bar{b}$ partial width of Z are combined with low energy constraints from $\Gamma(b \to s\gamma)$, $\Gamma(b \to c\tau\bar{\nu})$, and $B^0 - \bar{B}^0$ mixing to determine the experimentally favored configurations of THDM. This combination of observables rules out small charged Higgs boson masses and small values of $\tan\beta$. The configurations of THDM where the charged Higgs boson is much heavier or much lighter than the neutral Higgs bosons are ruled out also [21]. We assume $m_{H^0} = 100$ GeV, $m_{h^0} = m_{A^0} = 150$ GeV, and choose the other parameters restrictly within the bounds in Eq. (26) and the constraints of the literature [21].

In Fig. 5 we present the plot of the differential cross section of $\gamma\gamma \to H^+H^-$ versus the angle between the incoming photons and the positive charged Higgs boson with $m_{H^\pm} = 150$ GeV. The curve for the differential cross section at the lowest level is relatively flat, but the results with the $O(\alpha m_t^2/m_W^2)$ electroweak effects are strongly related to the angle θ. The figure shows there are large corrections near the positions when θ have values of zero and π. That means the charged Higgs pairs are dominantly produced in the forward and backward directions. This very dramatic change of the differential cross section of $\gamma\gamma \to H^+H^-$, when going from the lowest order calculation to including the Yukawa corrections, shows

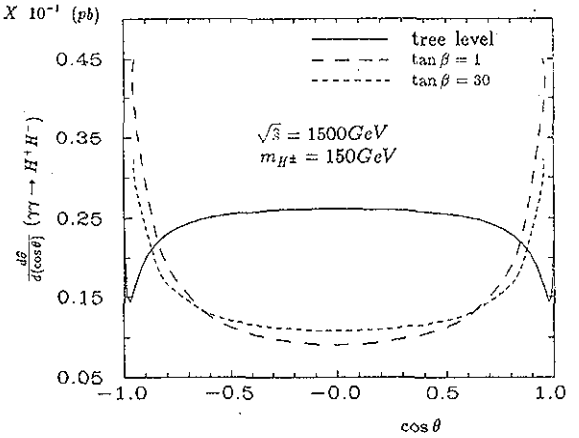

FIG. 5. The differential cross section as angular function between one of the incoming photons and the positive charged Higgs boson for subprocess $\gamma\gamma \to H^+H^-$ when $m_{H^\pm} = 150$ GeV. The full line is for the Born approximation. The long-dashed and short-dashed lines are the curves including $O(\alpha m_t^2/m_W^2)$ Yukawa corrections with $\tan\beta = 1$ and $\tan\beta = 30$, respectively.

that for the charged Higgs boson with intermediate mass is most feasible for detecting the charged Higgs pair in the forward and backward regions. The corrections with $\tan\beta = 1$ are larger than with $\tan\beta = 30$. It is because all the Yukawa correction form factors are directly proportional to a factor $g_+^2 + g_-^2$ (see the equations in the Appendix) and when $\tan\beta = 1$ that the coupling strength of H^+tb is stronger than when $\tan\beta = 30$ [see Eq. (8)]. In Fig. 6(a) the quantum corrections for a cross section for charged Higgs pair production in photon-photon mode are plotted as functions of center-of-mass $\sqrt{\hat{s}}$ with $m_{H^\pm} = 150$ GeV. Their relative corrections δ versus $\sqrt{\hat{s}}$ are depicted in Fig. 6(b), where the relative correction δ is defined as

$$\delta = \frac{\hat{\sigma} - \hat{\sigma}_0}{\hat{\sigma}_0} .$$

These relative corrections δ as functions of the ratio of vacuum expectation values $\tan\beta$ are shown in Fig. 6(c). The full line, long-dashed line, and short-dashed line are for $\sqrt{\hat{s}} = 1500$, 1000, and 400 GeV respectively.

Figures 6(a) and 6(b) show that the EW correction increases the total cross section of subprocess $\gamma\gamma \to H^+H^-$ when the center-of-mass energy $\sqrt{\hat{s}} \gg 1$ TeV, but decreases the cross section when $\sqrt{\hat{s}} \ll 1$ TeV. As a consequence of the coupling strength, with the ratio of vacuum values $\tan\beta = 1$, the absolute corrections are larger than with $\tan\beta = 30$. One can read out from Fig. 6(b) that, for $m_{H^\pm} = 150$ GeV and $\tan\beta = 1$, the effects of $O(\alpha m_t^2/m_W^2)$ Yukawa corrections may make a 33% increment in the cross section when $\sqrt{\hat{s}}$ approaches 2 TeV, but only a 23% reduction when $\sqrt{\hat{s}}$ is 400 GeV. Figure 6(c) shows that the corrections depends strongly on the value of $\tan\beta$ when $\sqrt{\hat{s}}$ is far away from the 1 TeV-energy region, but the dependence on the $\tan\beta$ becomes weak and

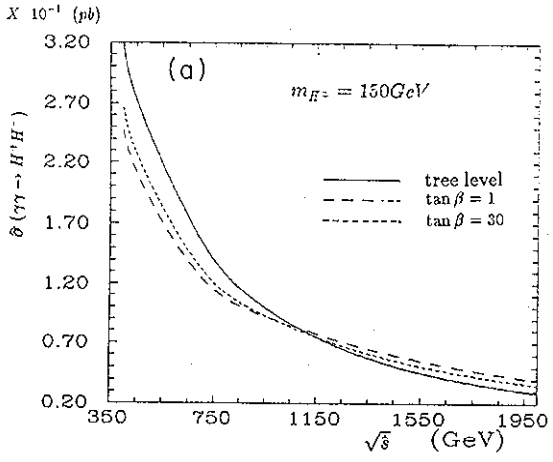

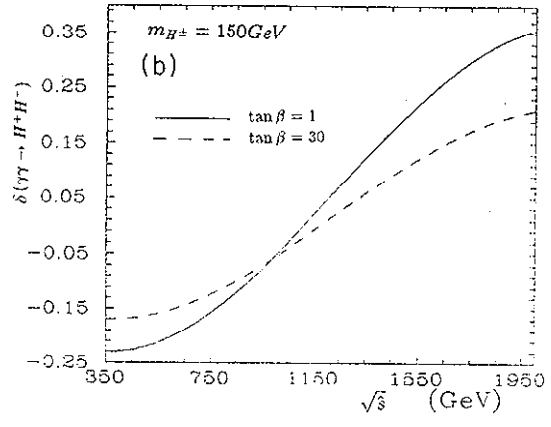

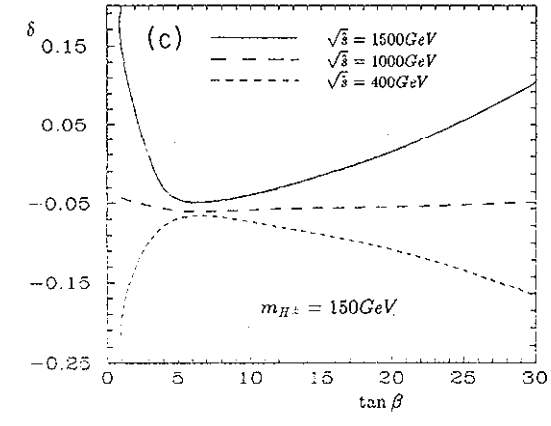

FIG. 6. (a) The total cross section of subprocess $\gamma\gamma \to H^+H^-$ versus center-of-mass energy $\sqrt{\hat{s}}$ with $m_{H^\pm} = 150$ GeV. The full line is for the Born approximation. The long-dashed and short-dashed lines are the cross sections including $O(\alpha m_t^2/m_W^2)$ Yukawa corrections with tanβ = 1 and tanβ = 30, respectively. (b) The relative correction δ of subprocess $\gamma\gamma \to H^+H^-$ versus center-of-mass energy $\sqrt{\hat{s}}$ with $m_{H^\pm} = 150$ GeV. The full line is for tanβ = 1 and the dashed line is of tanβ = 30. (c) The relative correction δ of subprocess $\gamma\gamma \to H^+H^-$ versus tanβ with $m_{H^\pm} = 150$ GeV. The full line is for $\sqrt{\hat{s}} = 1500$ GeV and the long-dashed line and short-dashed line correspond to $\sqrt{\hat{s}} = 1000$ GeV and $\sqrt{\hat{s}} = 400$ GeV, respectively.

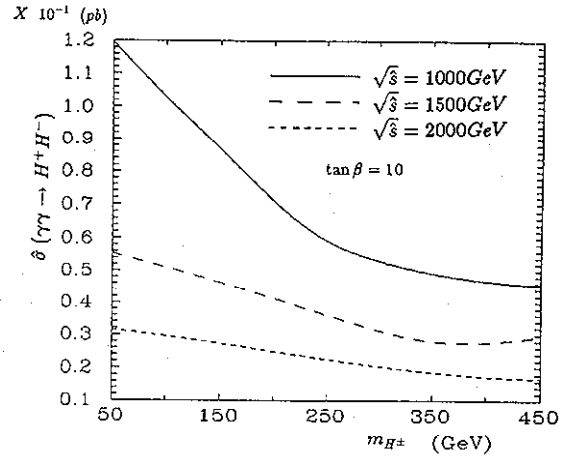

FIG. 7. The cross section including $O(\alpha m_t^2/m_W^2)$ Yukawa corrections of subprocess $\gamma\gamma \to H^+H^-$ versus the charged Higgs mass $m_{H^\pm}$. The full line is for $\sqrt{\hat{s}} = 1000$ GeV. The long-dashed and short-dashed lines correspond to $\sqrt{\hat{s}} = 1500$ GeV and $\sqrt{\hat{s}} = 2000$ GeV, respectively. (tanβ = 10.)

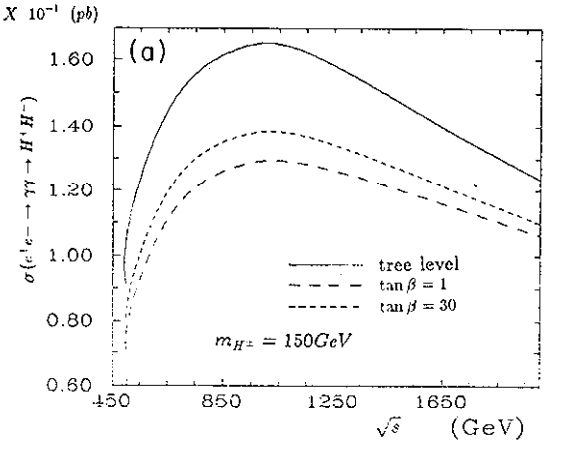

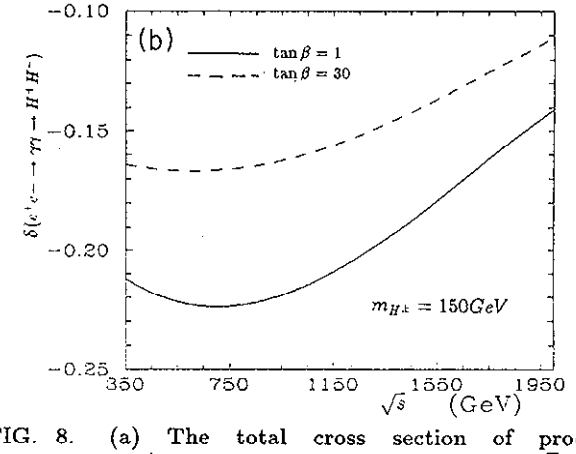

FIG. 8. (a) The total cross section of process $e^+e^- \to \gamma\gamma \to H^+H^-$ versus center-of-mass energy $\sqrt{\hat{s}}$ with $m_{H^\pm} = 150$ GeV. The full line is for the Born approximation. The long-dashed and short-dashed lines are the cross sections including $O(\alpha m_t^2/m_W^2)$ Yukawa corrections with tanβ = 1 and tanβ = 30, respectively. (b) The relative correction δ of process $e^+e^- \to \gamma\gamma \to H^+H^-$ versus center-of-mass energy $\sqrt{\hat{s}}$ with $m_{H^\pm} = 150$ GeV. The full line is for tanβ = 1 and the dashed line is for tanβ = 30.

the correction effects becomes smaller when $\sqrt{\hat{s}}$ has values around 1 TeV. This character is coincident with that in Figs. 6(a) and 6(b).

The dependence of the subprocess $\gamma\gamma \to H^+H^-$ cross section with Yukawa corrections on the charged Higgs boson masses are shown in Fig. 7. The production cross sections decrease when the charged Higgs boson mass becomes larger or the center-of-mass energy $\sqrt{\hat{s}}$ goes up.

The total cross section and relative corrections of process $e^+e^- \to\gamma\gamma \to H^+H^-$ versus the center-of-mass energy $\sqrt{s}$ with $m_{H^\pm} = 150$ GeV are depicted in Fig. 8(a) and 8(b) respectively. We can see that all the $O(\alpha m_t^2/m_W^2)$ Yukawa corrections decrease the production rate for both $\tan\beta = 1$ and $\tan\beta = 30$. The corrections with $\tan\beta = 1$ are more significant than with $\tan\beta = 30$. The correction can make as large as 22% reduction of the total cross section when $\tan\beta = 1$. This means that, in the process of charged Higgs pair production via photon-photon collision, we have to consider the radiative corrections.

IV. SUMMARY

In conclusion, we have calculated the $O(\alpha m_t^2/m_W^2)$ Yukawa corrections to the process of $e^+e^- \to\gamma\gamma \to H^+H^-$ in the e^+e^- collider. In the G_F-scheme, the corrections imply typically a few to 22 percent reduction of the total cross section of the tree level when $m_{H^\pm} = 150$ GeV. The corrections to the subprocess of $\gamma\gamma \to H^+H^-$, though, can be positive or negative, depending on the center-of-mass energy $\sqrt{\hat{s}}$. The dependence of the correction effects on the ratio of the vacuum expectation values comes from the behavior of the coupling strength of g_{H^+tb}.

ACKNOWLEDGMENTS

This work was supported in part by the National Natural Science Foundation of China and the National Committee of Science and Technology of China.

APPENDIX

The form factors corresponding to the loop diagrams in Figs. 3 and 4, are listed explicitly as

$$\begin{aligned} f_{1\mu} = {} & \frac{D}{8\pi^2}(g_+^2+g_-^2)([-p_{3\mu}B_0+(p_{2\mu}-p_{3\mu}-p_{4\mu})B_1][(p_2-p_3-p_4)^2,m_t^2,m_t^2] \\ & +\{(m_t^2p_{2\mu}+(m_{H^\pm}^2-2p_1\cdot p_3)p_{3\mu}-m_t^2p_{4\mu})C_{11} \\ & +[(m_{H^\pm}^2-m_t^2)p_{2\mu}+(m_t^2-m_{H^\pm}^2+2p_1\cdot p_3)p_{3\mu}+(m_t^2-m_{H^\pm}^2)p_{4\mu}]C_{12}\} \\ & \times[(p_4-p_2)^2,(p_2-p_3-p_4)^2,m_b^2,m_t^2,m_t^2]) \ , \end{aligned}$$

$$\begin{aligned} f_{2\mu} = {} & \frac{D}{8\pi^2}(g_+^2+g_-^2)([(p_{2\mu}-p_{3\mu})B_0+(p_{2\mu}-p_{3\mu}-p_{4\mu})B_1][(p_3+p_4-p_2)^2,m_t^2,m_t^2] \\ & +\{(m_{H^\pm}^2(p_{3\mu}-p_{2\mu})-m_t^2p_{4\mu})C_{11}+[(p_{2\mu}-p_{3\mu})(m_{H^\pm}^2-m_t^2)+p_{4\mu}(m_t^2-m_{H^\pm}^2+2p_1\cdot p_4)]C_{12}\} \\ & \times[p_4^2,(p_3+p_4-p_1)^2,m_b^2,m_t^2,m_t^2]) \ , \end{aligned}$$

$$\begin{aligned} f_{3\nu} = {} & \frac{D}{8\pi^2}(g_+^2+g_-^2)([(p_{4\mu}-p_{2\nu})B_0-p_{2\nu}B_1][p_2^2,m_t^2,m_t^2] \\ & +\{[m_{H^\pm}^2p_{2\nu}-(m_{H^\pm}^2+m_t^2)p_{4\mu}]C_{11}+[(m_t^2-m_{H^\pm}^2)p_{2\nu}+2(p_1\cdot p_3)p_{4\nu}]C_{12}\}[p_4^2,p_2^2,m_b^2,m_t^2,m_b^2]) \ , \end{aligned}$$

$$\begin{aligned} f_{4\nu} = {} & \frac{D}{8\pi^2}(g_+^2+g_-^2)(-[p_{3\nu}B_0+p_{2\nu}B_1][p_2^2,m_t^2,m_t^2] \\ & +\{[p_{3\nu}(m_{H^\pm}^2+m_t^2-2p_1\cdot p_4)-p_{2\nu}m_t^2]C_{11} \\ & [p_{2\nu}(m_t^2-m_{H^\pm}^2)+2p_1\cdot p_4p_{3\nu}]C_{12}\}[(p_2-p_3)^2,p_2^2,m_b^2,m_t^2,m_t^2]) \ , \end{aligned}$$

$$\begin{aligned} f_{5\mu} = {} & \frac{D}{16\pi^2}(g_+^2+g_-^2)([(p_{4\mu}-p_{2\mu})B_0+(p_{3\mu}+p_{4\mu}-p_{2\mu})B_1][(p_3+p_4-p_2)^2,m_b^2,m_b^2] \\ & +\{m_t^2(p_{2\mu}+p_{3\mu}-p_{4\mu})C_0+[m_{H^\pm}^2(p_{2\mu}-p_{4\mu})+m_t^2p_{3\mu}]C_{11} \\ & +[(m_t^2-m_{H^\pm}^2)p_{2\mu}+(m_{H^\pm}^2-m_t^2-2p_1\cdot p_3)p_{3\mu}+(m_{H^\pm}^2-m_t^2)p_{4\mu}]C_{12}\} \\ & \times[p_3^2,(p_3+p_4-p_2)^2,m_t^2,m_b^2,m_b^2]) \ , \end{aligned}$$

$$\begin{aligned} f_{6\mu} = {} & \frac{D}{16\pi^2}(g_+^2+g_-^2)([p_{4\mu}B_0+(p_{3\mu}+p_{4\mu}-p_{2\mu})B_1][(p_2-p_3-p_4)^2,m_b^2,m_b^2] \\ & +\{m_t^2(p_{3\mu}-p_{4\mu}-p_{2\mu})C_0+[m_t^2(p_{3\mu}-p_{2\mu})+(2p_1\cdot p_4-m_{H^\pm}^2)p_{4\mu}]C_{11} \\ & +[(p_{2\mu}-p_{3\mu})(m_t^2-m_{H^\pm}^2)+p_{4\mu}(m_{H^\pm}^2-m_t^2-2p_1\cdot p_4)]C_{12}\} \\ & \times[(p_3-p_2)^2,(p_2-p_3-p_4)^2,m_t^2,m_b^2,m_b^2]) \ , \end{aligned}$$

$$f_{7\nu} = \frac{D}{16\pi^2}(g_+^2+g_-^2)((p_{4\nu}B_0+p_{2\nu}B_1)[p_2^2,m_b^2,m_b^2]$$
$$+\{m_t^2(p_{2\nu}-p_{4\nu})C_0+[m_t^2p_{2\nu}+(2p_1\cdot p_3-m_t^2-m_{H^\pm}^2)p_{4\nu}]C_{11}$$
$$+[(m_{H^\pm}^2-m_t^2)p_{2\nu}-2p_1\cdot p_3p_{4\nu}]C_{12}\}[(p_2-p_4)^2,p_2^2,m_t^2,m_b^2,m_b^2])\ ,$$

$$f_{8\nu} = \frac{D}{16\pi^2}(g_+^2+g_-^2)(-[p_{3\nu}B_0+p_{2\nu}B_1][p_2^2,m_b^2,m_b^2]$$
$$+\{m_t^2(2p_{3\nu}-p_{2\nu})C_0+[p_{3\nu}(m_{H^\pm}^2+m_t^2-2p_1\cdot p_4)-m_t^2p_{2\nu}]C_{11}$$
$$+[p_{2\nu}(m_t^2-m_{H^\pm}^2)+2p_1\cdot p_4p_{3\nu}]C_{12}\}[(p_2-p_3)^2,p_2^2,m_t^2,m_b^2,m_b^2])\ ,$$

$$f_9 = \frac{D}{96\pi^2}(g_+^2+g_-^2)(-4B_0[p_1^2,m_b^2,m_b^2]+[(4m_t^2+4m_{H^\pm}^2-\hat{s}-2p_1\cdot p_3)C_0$$
$$+(3\hat{s}-6p_1\cdot p_3-4p_1\cdot p_4)C_{11}+2(2p_1\cdot p_3+p_1\cdot p_4)C_{12}+2(2p_1\cdot p_3-\hat{s}+2p_1\cdot p_4)C_{21}$$
$$-4(p_1\cdot p_3+p_1\cdot p_4)C_{23}+8C_{24}][(p_1-p_3-p_4)^2,p_1^2,m_b^2,m_b^2,m_b^2]$$
$$+\{(-4m_t^4-8m_t^2m_{H^\pm}^2+3\hat{s}m_t^2+2p_1\cdot p_3m_t^2-2p_1\cdot p_4m_t^2)D_0$$
$$+2(-m_{H^\pm}^4-7m_t^2m_{H^\pm}^2+\hat{s}m_t^2+p_1\cdot p_3m_{H^\pm}^2-p_1\cdot p_4m_t^2)D_{11}$$
$$+(\hat{s}m_{H^\pm}^2+3\hat{s}m_t^2-2p_1\cdot p_3(m_{H^\pm}^2-3m_t^2)-4p_1\cdot p_4(m_{H^\pm}^2+2m_t^2)+4p_1\cdot p_3p_1\cdot p_4)D_{12}$$
$$+2[(m_{H^\pm}^2+5m_t^2)p_1\cdot p_4-2p_1\cdot p_3m_t^2-2p_1\cdot p_3p_1\cdot p_4]D_{13}+(2m_{H^\pm}^4+2m_t^2m_{H^\pm}^2-\hat{s}m_{H^\pm}^2)D_{21}$$
$$+2[-\hat{s}m_{H^\pm}^2+\hat{s}m_t^2+2(m_{H^\pm}^2-m_t^2)p_1\cdot p_3+2p_1\cdot p_4m_{H^\pm}^2$$
$$-2p_1\cdot p_4m_t^2-2p_1\cdot p_3p_1\cdot p_4]D_{22}-4p_1\cdot p_3p_1\cdot p_4D_{23}$$
$$+2(\hat{s}m_{H^\pm}^2-\hat{s}m_t^2-2p_1\cdot p_3m_{H^\pm}^2+2p_1\cdot p_4m_t^2)D_{24}$$
$$+4(p_1\cdot p_3m_{H^\pm}^2-p_1\cdot p_4m_t^2)D_{25}$$
$$+4((m_t^2-m_{H^\pm}^2)p_1\cdot p_3-(m_{H^\pm}^2-m_t^2)p_1\cdot p_4+2p_1\cdot p_3p_1\cdot p_4)D_{26}$$
$$+2(2m_{H^\pm}^2-4m_t^2-\hat{s})D_{27}\}[p_4^2,(p_1-p_3-p_4)^2,p_1^2,m_t^2,m_b^2,m_b^2,m_b^2])\ ,$$

$$f_{10} = \frac{D}{48\pi^2}(g_+^2+g_-^2)(-2B_0[p_2^2,m_b^2,m_b^2]+[(2m_{H^\pm}^2+2m_t^2-\tfrac{1}{2}\hat{s}-p_1\cdot p_4)C_0$$
$$+(\tfrac{3}{2}\hat{s}-2p_1\cdot p_3-3p_1\cdot p_4)C_{11}+(p_1\cdot p_3+2p_1\cdot p_4)C_{12}+(2p_1\cdot p_3-\hat{s}+2p_1\cdot p_4)C_{21}$$
$$-2(p_1\cdot p_3+p_1\cdot p_4)C_{23}+4C_{24}][(p_2-p_3-p_4)^2,p_2^2,m_b^2,m_b^2,m_b^2]$$
$$-\{[4m_t^2m_{H^\pm}^2+2m_t^2-\tfrac{3}{2}\hat{s}m_t^2+m_t^2(p_1\cdot p_3-p_1\cdot p_4)]D_0$$
$$+(\hat{s}m_t^2-m_{H^\pm}^4-7m_t^2m_{H^\pm}^2-p_1\cdot p_3m_t^2+p_1\cdot p_4m_{H^\pm}^2)D_{11}$$
$$+(\tfrac{1}{2}\hat{s}m_{H^\pm}^2+\tfrac{3}{2}\hat{s}m_t^2-2p_1\cdot p_3m_{H^\pm}^2-4p_1\cdot p_3m_t^2-p_1\cdot p_4m_{H^\pm}^2$$
$$+3p_1\cdot p_4m_t^2+2p_1\cdot p_3p_1\cdot p_4)D_{12}+[(m_{H^\pm}^2+5m_t^2)p_1\cdot p_3-2p_1\cdot p_4(m_t^2+p_1\cdot p_3)]D_{13}$$
$$+(m_{H^\pm}^4+m_t^2m_{H^\pm}^2-\tfrac{1}{2}\hat{s}m_{H^\pm}^2)D_{21}$$
$$+[\hat{s}(m_t^2-m_{H^\pm}^2)+2(m_{H^\pm}^2-m_t^2)p_1\cdot p_3+2p_1\cdot p_4(m_{H^\pm}^2-m_t^2-p_1\cdot p_3)]D_{22}$$
$$-2(p_1\cdot p_3)(p_1\cdot p_4)D_{23}+[\hat{s}(m_{H^\pm}^2-m_t^2)+2p_1\cdot p_3m_t^2-2p_1\cdot p_4m_{H^\pm}^2]D_{24}$$
$$+2(p_1\cdot p_4m_{H^\pm}^2-p_1\cdot p_3m_t^2)D_{25}$$
$$+2[(m_t^2-m_{H^\pm}^2)p_1\cdot p_3+(m_t^2-m_{H^\pm}^2+2p_1\cdot p_3)p_1\cdot p_4]D_{26}$$
$$+(2m_{H^\pm}^2-4m_t^2-\hat{s})D_{27}\}[p_4^2,(p_2-p_3-p_4)^2,p_2^2,m_t^2,m_b^2,m_b^2,m_b^2])\ ,$$

$$f_{11} = \frac{D}{24\pi^2}(g_+^2+g_-^2)(-4B_0[p_1^2,m_t^2,m_t^2]+[(4m_{H^\pm}^2-\hat{s}-2p_1\cdot p_3)C_0$$
$$+(3\hat{s}-6p_1\cdot p_3-4p_1\cdot p_4)C_{11}+(4p_1\cdot p_3+2p_1\cdot p_4)C_{12}$$
$$+2(2p_1\cdot p_3-\hat{s}+2p_1\cdot p_4)C_{21}-4(p_1\cdot p_3+p_1\cdot p_4)C_{23}$$
$$+8C_{24}][(p_1-p_3-p_4)^2,p_1^2,m_t^2,m_t^2,m_t^2]$$
$$+\{(6m_t^2m_{H^\pm}^2-2m_{H^\pm}^4-\hat{s}m_t^2+2p_1\cdot p_3m_{H^\pm}^2-2p_1\cdot p_4m_t^2)D_{11}$$
$$+[\hat{s}m_{H^\pm}^2-\hat{s}m_t^2-2(p_1\cdot p_3+2p_1\cdot p_4)m_{H^\pm}^2+2(3m_t+2p_1\cdot p_3)p_1\cdot p_4]D_{12}$$
$$+2(p_1\cdot p_3m_t^2+p_1\cdot p_4m_{H^\pm}^2-2m_t^2p_1\cdot p_4-2p_1\cdot p_3p_1\cdot p_4)D_{13}$$
$$+(2m_{H^\pm}^4+2m_t^2m_{H^\pm}^2-\hat{s}m_{H^\pm}^2)D_{21}$$

$$
\begin{aligned}
&+2[\hat{s}m_t^2-\hat{s}m_{H^\pm}^2+2(m_{H^\pm}^2-m_t^2)(p_1\cdot p_3+p_1\cdot p_4)-2(p_1\cdot p_3)(p_1\cdot p_4)]D_{22}\\
&-4(p_1\cdot p_3)(p_1\cdot p_4)D_{23}+2(\hat{s}m_{H^\pm}^2-\hat{s}m_t^2+2p_1\cdot p_4m_t^2-2p_1\cdot p_3m_{H^\pm}^2)D_{24}\\
&+4(p_1\cdot p_3m_{H^\pm}^2-p_1\cdot p_4m_t^2)D_{25}\\
&+4[(m_t^2-m_{H^\pm}^2)(p_1\cdot p_3+p_1\cdot p_4)+2(p_1\cdot p_3)(p_1\cdot p_4)]D_{26}\\
&+2(2m_{H^\pm}^2-4m_t^2-\hat{s})D_{27}\}[p_4^2,(p_1-p_3-p_4)^2,p_1^2,m_b^2,m_t^2,m_t^2,m_t^2])\ ,
\end{aligned}
$$

$$
\begin{aligned}
f_{12}=&\frac{D}{12\pi^2}(g_+^2+g_-^2)(-2B_0[(p_2-p_3-p_4)^2,m_t^2,m_t^2]\\
&+[(2m_{H^\pm}^2-\hat{s}+p_1\cdot p_3)C_0+p_1\cdot p_3C_{11}+(\tfrac{1}{2}\hat{s}+p_1\cdot p_4)C_{12}\\
&+(2p_1\cdot p_3+2p_1\cdot p_4-\hat{s})C_{22}+2(p_1\cdot p_4-p_1\cdot p_3)C_{23}\\
&+4C_{24}][p_2^2,(p_2-p_3-p_4)^2,m_t^2,m_t^2,m_t^2]\\
&+\{(3m_{H^\pm}^2m_t^2-m_{H^\pm}^4+\tfrac{1}{2}\hat{s}m_{H^\pm}^2-\hat{s}m_t^2-m_{H^\pm}^2p_1\cdot p_3+m_t^2p_1\cdot p_4)D_{11}\\
&+[p_1\cdot p_3(2m_t^2-m_{H^\pm}^2)+p_1\cdot p_4(2p_1\cdot p_3-m_t^2)D_{12}\\
&+[\tfrac{1}{2}\hat{s}(m_t^2-m_{H^\pm}^2)+p_1\cdot p_3(2m_{H^\pm}^2-3m_t^2)+p_1\cdot p_4(m_{H^\pm}^2-2p_1\cdot p_3)]D_{13}\\
&+(m_{H^\pm}^4+m_{H^\pm}^2m_t^2-\tfrac{1}{2}\hat{s}m_{H^\pm}^2)D_{21}-2p_1\cdot p_3p_1\cdot p_4D_{22}\\
&+[(\hat{s}-2p_1\cdot p_3)(m_t^2-m_{H^\pm}^2)+2p_1\cdot p_4(m_{H^\pm}^2-m_t^2-p_1\cdot p_3))D_{23}\\
&+2(m_{H^\pm}^2p_1\cdot p_3-m_t^2p_1\cdot p_4)D_{24}+[\hat{s}(m_{H^\pm}^2-m_t^2)-2m_{H^\pm}^2p_1\cdot p_3+2m_t^2p_1\cdot p_4]D_{25}\\
&+2[p_1\cdot p_3(m_t^2-m_{H^\pm}^2)+p_1\cdot p_4(m_t^2-m_{H^\pm}^2+2p_1\cdot p_3)]D_{26}\\
&+(2m_{H^\pm}^2-4m_t^2-\hat{s})D_{27}\}[p_3^2,p_2^2,(p_2-p_3-p_4)^2,m_b^2,m_t^2,m_t^2,m_t^2])\ ,
\end{aligned}
$$

$$
\begin{aligned}
f_{13}=&\frac{D}{48\pi^2}(g_+^2+g_-^2)(-4B_0[p_3^2,m_b^2,m_t^2]+[(\hat{s}-2m_{H^\pm}^2-4p_1\cdot p_3)C_0+4(\hat{s}-3p_1\cdot p_3-3p_1\cdot p_4)C_{11}\\
&+2(4p_1\cdot p_3-\hat{s})C_{12}][(p_1-p_3-p_4)^2,p_3^2,m_b^2,m_b^2,m_t^2]+\{2m_t^2(2p_1\cdot p_3-3p_1\cdot p_4)D_0\\
&+(\hat{s}m_t^2-12m_t^2m_{H^\pm}^2+4p_1\cdot p_3m_{H^\pm}^2-6p_1\cdot p_4m_t^2)D_{11}\\
&+[4\hat{s}m_t^2+2p_1\cdot p_3(4m_t^2-\hat{s})-4p_1\cdot p_4(m_t^2-p_1\cdot p_3)]D_{12}\\
&+[12m_t^2m_{H^\pm}^2-5\hat{s}m_t^2-(4m_{H^\pm}^2+6m_t^2-2\hat{s})p_1\cdot p_3]D_{13}+(\hat{s}m_{H^\pm}^2-2m_{H^\pm}^4-2m_t^2m_{H^\pm}^2)D_{21}\\
&+2[\hat{s}m_{H^\pm}^2-\hat{s}m_t^2-2p_1\cdot p_3(m_{H^\pm}^2-m_t^2)-2(m_{H^\pm}^2-m_t^2-p_1\cdot p_3)p_1\cdot p_4]D_{22}\\
&+(\hat{s}m_{H^\pm}^2-2m_{H^\pm}^4-2m_t^2m_{H^\pm}^2)D_{23}+2(\hat{s}m_t^2-\hat{s}m_{H^\pm}^2+2p_1\cdot p_3m_{H^\pm}^2-2p_1\cdot p_4m_t^2)D_{24}\\
&+2(2m_{H^\pm}^4+2m_t^2m_{H^\pm}^2-\hat{s}m_t^2)D_{25}+2(\hat{s}m_t^2-\hat{s}m_{H^\pm}^2-2m_t^2p_1\cdot p_3+2p_1\cdot p_4m_{H^\pm}^2)D_{26}\\
&+2(4m_t^2-2m_{H^\pm}^2+\hat{s})D_{27}\}[p_4^2,(p_1-p_3-p_4)^2,p_3^2,m_t^2,m_b^2,m_b^2,m_t^2])\ ,
\end{aligned}
$$

$$
\begin{aligned}
f_{14}=&\frac{D}{48\pi^2}(g_+^2+g_-^2)(-4B_0[p_3^2,m_t^2,m_b^2]+[(\hat{s}-2m_{H^\pm}^2-4p_1\cdot p_3)C_0\\
&+4(\hat{s}-3p_1\cdot p_3-3p_1\cdot p_4)C_{11}+2(4p_1\cdot p_3-\hat{s})C_{12}][(p_3+p_4-p_1)^2,p_3^2,m_t^2,m_t^2,m_b^2]\\
&+\{2(2p_1\cdot p_3m_{H^\pm}^2+p_1\cdot p_4m_t^2)D_{11}-2[(m_t^2+\hat{s})p_1\cdot p_3+(m_t^2-2p_1\cdot p_3)p_1\cdot p_4]D_{12}\\
&+2p_1\cdot p_3(m_t^2-2m_{H^\pm}^2+\hat{s})D_{13}+(-2m_{H^\pm}^4-2m_t^2m_{H^\pm}^2+\hat{s}m_{H^\pm}^2)D_{21}\\
&+2[\hat{s}m_{H^\pm}^2-\hat{s}m_t^2+2p_1\cdot p_3(m_t^2-m_{H^\pm}^2)+2p_1\cdot p_4(m_t^2-m_{H^\pm}^2+p_1\cdot p_3)]D_{22}\\
&+(\hat{s}m_{H^\pm}^2-2m_{H^\pm}^4-2m_t^2m_{H^\pm}^2)D_{23}+(2\hat{s}m_t^2-2\hat{s}m_{H^\pm}^2+4p_1\cdot p_3m_{H^\pm}^2-4p_1\cdot p_4m_t^2)D_{24}\\
&+2(2m_{H^\pm}^4+2m_t^2m_{H^\pm}^2-\hat{s}m_t^2)D_{25}+2(\hat{s}m_t^2-\hat{s}m_{H^\pm}^2-2p_1\cdot p_3m_t^2+2p_1\cdot p_4m_{H^\pm}^2)D_{26}\\
&+2(4m_t^2-2m_{H^\pm}^2+\hat{s})D_{27}\}[p_4^2,(p_3+p_4-p_1)^2,p_3^2,m_b^2,m_t^2,m_t^2,m_b^2])\ ,
\end{aligned}
$$

where $D=4-2\epsilon$. The form factors f_i ($i=1$–8) correspond to the contributions of the diagrams in Figs. 3 and the f_i ($i=9$–14) to the diagrams in Fig. 4, respectively. The arguments of B, C, and D functions are written at the end of formulas in parentheses. Their definitions can be found in Ref. [10].

[1] P. W. Higgs, Phys. Lett. **12**, 132 (1964); **13**, 508 (1964); Phys. Rev. **145**, 1156 (1966); F. Englert and R. Brout, Phys. Rev. Lett. **13**, 321 (1964).

[2] G. S. Guralnik, C. R. Hagen, and T. W. B. Kibble, Phys. Rev. Lett. **13**, 585 (1964); T. W. B. Kibble, Phys. Rev. **155**, 1554 (1967).

[3] CDF Collaboration, F. Abe *et al.*, Phys. Rev. D **50**, 2966 (1994).

[4] J. Schwindling, in *Proceedings of the International Europhysics Conference on High Energy Physics*, Marseille, France, 1993, edited by J. Carr and M. Perrottet (Editions Frontieres, Gif-sur-Yvette, 1993).
[5] V. Barger and R. J. N. Phillips, Phys. Rev. D **39**, 3310 (1989); A. C. Bawa, C. S. Kim, and A. D. Martin, Z. Phys. C **47**, 75 (1990).
[6] J. F. Gunion, H. E. Haber, G. Kane, and S. Dawson, *The Higgs Hunters' Guide* (Addison Wesley, Reading, MA, 1990); H. E. Haber, in *Phenomenology of the Standard Model and Beyond*, edited by D. P. Roy and Probir Roy (World Scientific, Singapore, 1989).
[7] I. F. Ginzburg, G. L. Kotkin, V. G. Serbo, and V. I. Telnov, Pis'ma Z. Eksp. Teor. Fiz. **34**, 514 (1981); Nucl. Instrum. Methods **205**, 47 (1983).
[8] D. Bowser-Chao, K. Cheung, and S. Thomas, Phys. Lett. B **315**, 399 (1993).
[9] K. I. Aoki, Z. Hioki, R. Kawabe, M. Konuma, and T. Muta, Prog. Theor. Phys. **64**, 707 (1980); **65**, 1001 (1981); Prog. Theor. Phys. Suppl. **73**, 1 (1982).
[10] Gunion, Haber, Kane, and Dawson [6].
[11] A. Denner, Fortschr. Phys. **41**, 307 (1993).
[12] W. Hollik, Z. Phys. C **32**, 291 (1986).
[13] V. Telnov, Nucl. Instrum. Methods **A294**, 72 (1990); I. Ginzburg, G. Kotkin, and H. Spiesbergerm, Fortschr. Phys. **34**, 687 (1986).
[14] K. Cheung, Phys. Rev. D **47**, 3750 (1993).
[15] W. Hollik, Z. Phys. C **37**, 569 (1988).
[16] M. Bohm, W. Hollik, and H. Spiesburger, Fortschr. Phys. C **27**, 523 (1985).
[17] Particle Data Group, L. Montanet *et al.*, Phys. Rev. D **50**, 1173 (1994).
[18] ALEPH Collaboration, D. Decamp *et al.*, Phys. Rep. **216**, 253 (1992).
[19] G. G. Athanasiu, P. J. Franzini, and F. J. Gilman, Phys. Rev. D **32**, 3010 (1985); P. Krawczyk and S. Pokorski, Phys. Rev. Lett. **60**, 182 (1988); A. J. Buras, P. Krawczyk, M. E. Lautenbacher, and C. Salazar, Nucl. Phys. **B337**, 284 (1990); J. F. Gunion and B. Grzadkowski, Phys. Lett. B **243**, 301 (1990); D. Cocolicchoi and J.-R. Cudell, *ibid.* **245**, 591 (1990); V. Barger, J. L. Hewett, and R. J. N. Phillips, Phys. Rev. D **41**, 3421 (1990).
[20] A. Denner, Fortschr. Phys. **41**, 307 (1993).
[21] A. K. Grant, Phys. Rev. D **51**, 207 (1995).